

Photochemistry of Intramolecular Charge Transfer Excited States in Donor–Acceptor-Substituted Diamines

Yingsheng Wang and Kirk S. Schanze*

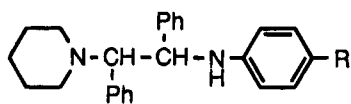
Department of Chemistry, University of Florida, Gainesville, Florida 32611-7200

Received: September 14, 1994; In Final Form: February 9, 1995[⊗]

The photochemistry and photophysics of 1,2-diamines $C_5H_{10}NCHPhCHPhNHC_6H_4R$ (**1**, $R = CN$, and **2**, $R = 4$ -pyridyl) have been examined. These compounds display a strong absorption band in the near-UV which is due to intramolecular charge transfer from the secondary amine group to the 4-cyanophenyl or (4-pyridyl)phenyl acceptor unit. Photoexcitation into this absorption band leads to moderately intense fluorescence from the 1LE state of the charge transfer chromophore and to homolytic bond fragmentation across the 1,2 C–C bond with moderate quantum efficiency. Detailed photochemical and photophysical studies reveal that the bond fragmentation reaction ensues from a second intramolecular charge transfer excited state (denoted 1CT) which is based on electron transfer from the tertiary piperidine nitrogen to the 4-cyanophenyl or (4-pyridyl)phenyl unit. Photochemical product analysis reveals that *erythro* \rightarrow *threo* (or *threo* \rightarrow *erythro*) isomerization occurs under both argon-degassed and air-saturated conditions. This observation indicates that recombination of the radicals formed by bond fragmentation occurs, both within the geminate pair and between free radicals that have escaped the solvent cage. Analysis of fluorescence, transient absorption, and steady-state photochemical kinetics data indicates that (1) internal conversion from the 1LE state to the 1CT state by intramolecular electron transfer occurs with $k \geq 10^9$ s $^{-1}$ in all of the diamines; (2) bond fragmentation within the 1CT state occurs with $k \geq 10^8$ s $^{-1}$ in each of the diamines; (3) bond fragmentation may be faster in *erythro*-**1** than in *threo*-**1**.

Introduction

Donor–acceptor-substituted molecules have attracted interest for decades. This interest has been motivated by the fact that donor–acceptor compounds display unique optical and photophysical properties owing to the charge transfer interaction between the electron donor and acceptor substituents.^{1–10} Recent interest in this area has increased substantially because donor–acceptor compounds possess a large hyperpolarizability, making them useful for the construction of organic or organometallic materials for nonlinear optical conversion.¹¹

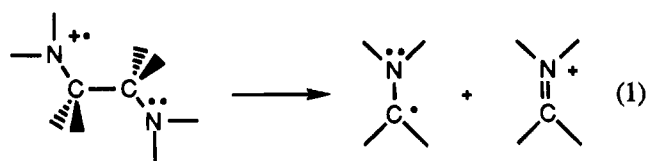


- 1** $R = -CN$
2 $R = 4$ -pyridyl

A variety of structurally related donor–acceptor-substituted compounds that contain the aminobenzonitrile (ABN) unit have been intensively investigated in an effort to elucidate the origin of the dual fluorescence that is characteristic of 4-(dimethylamino)benzonitrile (**8**, see Chart 1) and related ABN compounds.^{6,7,12,13} Several models have been developed to explain the dual fluorescence. Popular among them is the twisted intramolecular charge transfer (TICT) model, which attributes the high-energy fluorescence band to the normal locally excited (LE) π,π^* excited state of the ABN chromophore and the “anomalous” low-energy band to the TICT state in which

interaction between the amino donor and the benzonitrile acceptor is decoupled by out-of-plane twisting of the amino substituent.^{6,7} Despite the widespread use of the TICT model, more recent studies suggest that the dual fluorescence may be due to two energetically closely spaced excited states, one having a greater degree of CT character than the other but with neither having minimum overlap or “TICT” character.^{12,13}

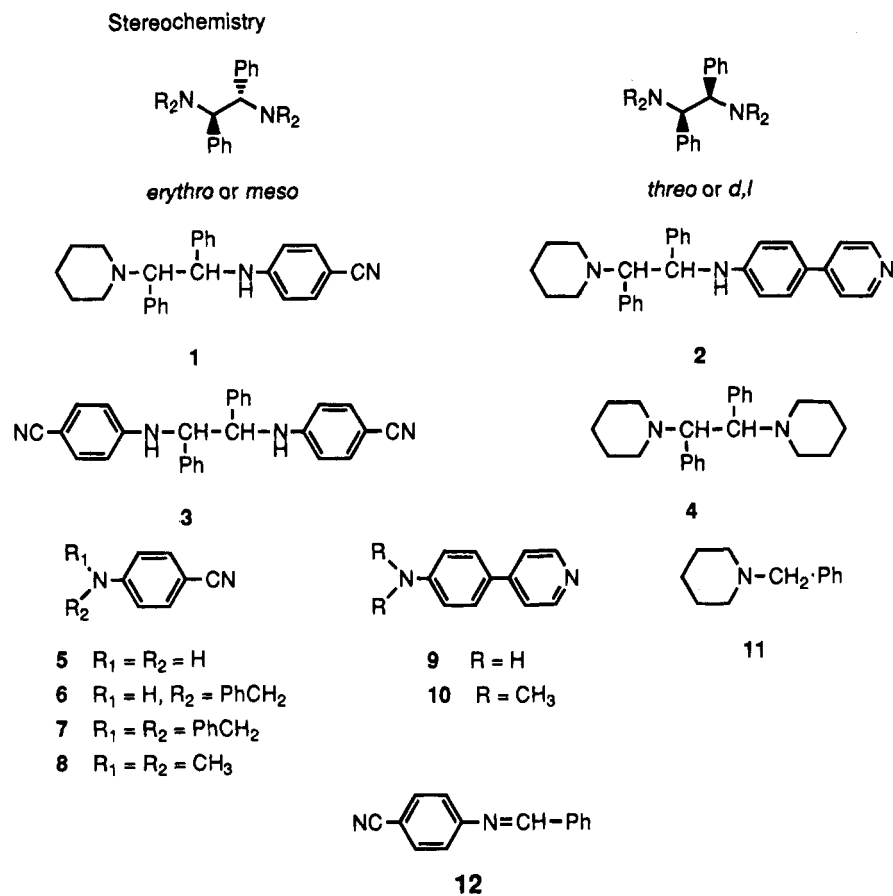
Throughout all of the studies that have been carried out to explore the excited-state properties of ABN-type and related donor–acceptor compounds, photophysical tools such as steady-state and time-resolved fluorescence and transient absorption spectroscopy have played the dominant role.^{1–13} We recently embarked on an effort to develop a *photochemical* probe that would provide a complementary means to examine the properties of intramolecular charge transfer excited states in a variety of donor–acceptor-substituted organic and organometallic compounds.^{14–16} Our approach relies upon the rapid C–C bond fragmentation reaction of 1,2-diamines that is triggered by single electron transfer oxidation, eq 1:



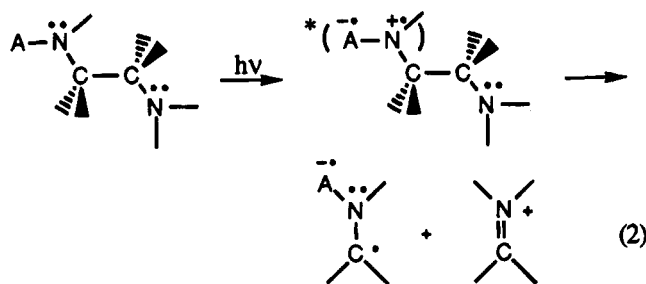
Studies by Whitten and co-workers indicate that, following oxidation, the radical cations of 1,2-diamines fragment with rates exceeding 10^9 s $^{-1}$.^{17,18} The rapidity of this C–C bond fragmentation reaction suggested to us that 1,2-diamines might serve as useful probes for the structure and dynamics of intramolecular charge transfer excited states in ABN and related

[⊗] Abstract published in *Advance ACS Abstracts*, April 15, 1995.

CHART 1



donor-acceptor-substituted compounds. Specifically, by incorporating one of the amine units of a 1,2-diamine into a donor-acceptor chromophore, it might be possible to trigger C-C bond fragmentation via excitation of the intramolecular charge transfer absorption, e.g.



A = an electron acceptor

Since the C-C bond fragmentation reaction must compete with decay of the charge transfer excited state, it should be possible to gain insight concerning the electronic structure and dynamics of the charge transfer state by studying the efficiency of the C-C bond fragmentation reaction. Of special interest in this regard would be to compare the reactivity of the LE and "TICT" excited states in diamines that incorporate the ABN chromophore.^{6,7,12,13}

The present paper presents the results of a detailed photochemical and photophysical study of a series of 1,2-diamines that incorporate the diamine into an intramolecular donor-acceptor chromophore (*e*-1, *t*-1, and *e*-2, see Chart 1). Photoexcitation of these diamines into the charge transfer absorption band triggers C-C bond fragmentation, with an efficiency that

depends upon the nature of the chromophore and the stereochemistry with respect to the diamine unit. Detailed photochemical and photophysical studies provide sufficient information to allow the development of a concise mechanism that encompasses both the nature of the excited states responsible for the photochemistry and the structure and reactivity of the reactive intermediates produced by C-C bond fission.

Experimental Section

General Synthetic Details. Reagent grade solvents and chemicals were used without purification unless otherwise noted. Silica gel (Merck, 230-400 mesh) and neutral alumina (Fisher, Brockman grade III) were used for chromatography. NMR spectra were run on either GE QE-300 MHz or Varian VXR-300 MHz spectrophotometers.

***erythro*-2-Piperidino-1,2-diphenylethanol (*e*-20).**¹⁹ A mixture of *trans*-stilbene oxide (2.94 g, 15 mmol), piperidine (12 mL, 10.3 g, 120 mmol), and *p*-toluenesulfonic acid (0.2 g, 1 mmol, as catalyst) was heated to reflux under a blanket of nitrogen. The reaction was monitored by TLC (silica, ethyl acetate-hexane 20:80 v/v). The reaction was stopped after 11 h of refluxing, when the *trans*-stilbene oxide spot ($R_f = 0.8$) had disappeared completely. Unreacted piperidine was removed under reduced pressure, and a white solid was obtained. The solid was dissolved in 50 mL of ethyl acetate and extracted with 1 M aqueous NaOH and then with H₂O. After the organic layer was dried with MgSO₄, the solvent was removed. Product *e*-20 was obtained as an off-white crystalline solid without further purification, yield 3.87 g (92%). TLC (silica, ethyl acetate-hexane 20:80 v/v): $R_f = 0.3-0.4$. ¹H NMR (300 MHz, CDCl₃): δ 1.5 (m, 2H, pip CH₂), 1.6 (m, 4H, pip CH₂), 2.5 (m, 2H, pip CH₂), 2.6 (m, 2H, pip CH₂), 3.39 (d, $J = 4.8$ Hz,

1H, benzylic), 3.53 (br, 1H, OH), 5.38 (d, $J = 4.8$ Hz, 1H, benzylic), 7.0–7.2 (m, 10H, phenyl). ^{13}C NMR (75 MHz, CDCl_3): δ 24.6, 26.3, 52.5 (all pip), 71.6 (benzylic), 76.5 (benzylic), 126.2, 126.6, 127.0, 127.4 (2C), 129.5, 136.7, 141.4 (all phenyls).

threo-2-Piperidino-1,2-diphenylethanol (*t*-20).¹⁹ The synthesis of this compound followed the same procedure as that for *e*-20 in 90% yield except that *cis*-stilbene oxide was used as the starting epoxide. TLC (silica, ethyl acetate–hexane 1:9 v/v): $R_f = 0.3$ –0.5. ^1H NMR (300 MHz, CDCl_3): δ 1.4 (m, 2H, pip CH_2), 1.7 (m, 4H, pip CH_2), 2.3 (m, 2H, pip CH_2), 2.7 (m, 2H, pip CH_2), 3.57 (d, $J = 10.5$ Hz, 1H, benzylic), 5.07 (d, $J = 10.5$ Hz, 1H, benzylic), 5.4 (br, 1H, OH), 7.1–7.3 (m, 10H, phenyl). ^{13}C NMR (75 MHz, CDCl_3): δ 24.3 (pip), 26.6 (pip), 50.3 (broad, pip), 70.4 (benzylic), 77.2 (benzylic), 127.3 (2C), 127.6, 127.7, 127.9, 129.9, 133.5, 141.8 (all phenyls).

erythro-1-((4-Cyanophenyl)amino)-2-piperidino-1,2-diphenylethane (*e*-1). A mixture of *e*-20 (562 mg, 2.0 mmol), 10 mL of freshly distilled CH_2Cl_2 , and triethylamine (0.8 mL, 6.0 mmol) was placed in a 100 mL three-necked round bottom flask, and the resulting solution was purged with N_2 for 30 min. During this period the temperature was adjusted to -20 °C by using a dry ice–2-propanol bath. A solution of methanesulfonyl chloride (0.155 mL, 2.0 mmol) dissolved in 2 mL of freshly distilled CH_2Cl_2 was added dropwise by using a syringe. The resulting mixture was maintained at -20 °C and stirred gently for 1 h. After this period of time a solution of 4-aminobenzonitrile (236 mg, 2.0 mmol) in 3 mL of freshly distilled CH_2Cl_2 was added dropwise by using a syringe. After the temperature of the solution increased to ambient temperature, the solution was heated to reflux. During the reflux period the reaction was monitored by TLC (silica, ethyl acetate–hexane 3:7 v/v, 4-aminobenzonitrile at $R_f = 0.2$, product at $R_f = 0.6$). Refluxing was discontinued after 16 h, at which point 4-aminobenzonitrile was no longer visible by TLC. The solvent was removed under reduced pressure, and the crude product was purified by chromatography (silica, ethyl acetate–hexane 15:85 v/v). Product *e*-1 was obtained as an off-white crystalline solid, yield 500 mg (66%). Mp: 115–116 °C. TLC (silica, ethyl acetate–hexane 5:95 v/v): $R_f = 0.2$. ^1H NMR (300 MHz, CDCl_3): δ 1.4–1.65 (m, 6H, pip), 2.35–2.55 (m, 4H, pip), 3.50 (d, $J = 5.7$ Hz, 1H, benzylic), 4.84 (d of d, $J_1 = 5.7$ Hz, $J_2 = 2.7$ Hz, 1H, benzylic, adjacent to NH), 5.48 (d, $J = 2.7$ Hz, 1H, NH), 6.47 (d, $J = 9.0$ Hz, 2H, benzonitrile), 6.9–7.0 (m, 4H, phenyl), 7.1–7.2 (m, 6H, phenyl), 7.31 (d, $J = 9.0$ Hz, 2H, benzonitrile). ^{13}C NMR (75 MHz, CDCl_3): δ 24.6, 26.2, 52.3 (all pip), 58.0 (benzylic), 75.3 (benzylic), 99.1, 113.6, 120.4, 127.0 (2C), 127.3, 127.7, 128.0, 128.9, 133.4, 137.0, 139.9, 151.0 (all aromatic). ^1H NMR (300 MHz, DMSO): δ 1.0–1.4 (m, 6H, pip), 1.91 (m, 2H, pip), 2.45 (m, 2H, pip), 3.77 (d, $J = 10.5$ Hz, 1H, benzylic), 5.19 (d of d, $J_1 = 10.5$ Hz, $J_2 = 8.7$ Hz, 1H, benzylic, adjacent to NH), 6.63 (d, $J = 8.4$ Hz, 2H, benzonitrile), 6.81 (d, $J = 8.7$ Hz, 1H, NH), 7.1–7.3 (m, 10H, phenyl), 7.43 (d, $J = 8.4$ Hz, 2H, benzonitrile). HRMS calcd for $\text{C}_{26}\text{H}_{28}\text{N}_3$ ($M + H$) 382.2283, found 382.2269.

threo-1-((4-Cyanophenyl)amino)-2-piperidino-1,2-diphenylethane (*t*-1). A mixture of *t*-20 (281 mg, 1.0 mmol), 5 mL of freshly distilled CH_2Cl_2 , and triethylamine (0.4 mL, 3.0 mmol) was placed in a 100 mL three-necked round bottom flask, and the resulting solution was purged with N_2 for 30 min. During this period the temperature was adjusted to -20 °C by using a dry ice–2-propanol bath. A solution of methanesulfonyl chloride (0.08 mL, 1.0 mmol) dissolved in 1 mL of freshly distilled CH_2Cl_2 was added dropwise by using a syringe. The resulting mixture was maintained at -20 °C and was stirred

gently for 1 h. After this period of time a solution of 4-aminobenzonitrile (118 mg, 1.0 mmol) in 2 mL of freshly distilled CH_2Cl_2 was added dropwise by using a syringe. After the temperature increased to ambient temperature, the solution was heated to reflux. During the reflux period the reaction was monitored by TLC (silica, ethyl acetate–hexane 3:7 v/v, 4-aminobenzonitrile at $R_f = 0.1$, product at $R_f = 0.7$). The reaction occurred very slowly under these conditions. The CH_2Cl_2 solvent was removed by evaporation under a slow stream of N_2 , whereupon 5 mL of 1,2-dichloroethane was added to the flask. The resulting dichloroethane solution was heated to reflux for 18 h. After this reflux period the solvent was removed by evaporation under reduced pressure and the crude product was purified by chromatography (silica, ethyl acetate–hexane 15:85 v/v). Product *t*-1 was obtained as an off-white crystalline solid, yield 180 mg (47%). Mp: 146–148 °C. TLC (silica, ethyl acetate–hexane 3:7 v/v): $R_f = 0.7$. ^1H NMR (300 MHz, CDCl_3): δ 1.39 (m, 2H, pip), 1.59 (m, 2H, pip), 1.68 (m, 2H, pip), 2.38 (m, 4H, pip), 3.64 (d, $J = 10.5$ Hz, 1H, benzylic), 4.63 (d, $J = 10.5$ Hz, 1H, benzylic), 6.53 (d, $J = 8.7$ Hz, 2H, benzonitrile), 6.72 (s, 1H, NH), 7.0–7.3 (m, 10H, phenyl), 7.34 (d, $J = 8.7$ Hz, 2H, benzonitrile). ^{13}C NMR (75 MHz, CDCl_3): δ 24.3, 26.7, 49.9 (br) (all pip), 57.7 (benzylic), 76.1 (benzylic), 99.0, 113.5, 120.4, 127.1, 127.3, 127.7, 127.7, 128.3, 129.8, 133.4, 141.1, 151.6 (all aromatic). ^1H NMR (300 MHz, DMSO): δ 1.23 (m, 2H, pip), 1.42 (m, 2H, pip), 1.56 (m, 2H, pip), 2.22 (m, 2H, pip), 2.29 (m, 2H, pip), 3.76 (d, $J = 10.8$ Hz, 1H, benzylic), 4.95 (d of d, $J_1 = 10.8$ Hz, $J_2 = 3.0$ Hz, 1H, benzylic, adjacent to NH), 6.67 (d, $J = 8.4$ Hz, 2H, benzonitrile), 6.92 (d, $J = 3.0$ Hz, 1H, NH), 7.0–7.3 (m, 10H, phenyl), 7.37 (d, $J = 8.4$ Hz, 2H, benzonitrile). HRMS calcd for $\text{C}_{26}\text{H}_{28}\text{N}_3$ ($M + H$) 382.2283, found 382.2327.

4-(*p*-Aminophenyl)pyridine (21). (a) *4-(p-Nitrophenyl)pyridine*.²⁰ A mixture of 4-phenylpyridine (3.1 g, 20 mmol), 10 mL of concentrated H_2SO_4 , and 1 mL of fuming HNO_3 was heated to 100 °C under a blanket of N_2 for 2 h. After being cooled to room temperature, the resulting mixture was poured into 100 g of ice to yield a yellow transparent solution. NH_4OH (5 M) was added to the solution, and at pH = 6 a copious amount of yellow precipitate formed. ^1H NMR (DMSO solution) of this solid shows that it is a mixture of the *o*-, *m*-, and *p*-isomers of 4-(nitrophenyl)pyridine. The mixture of isomers was dissolved in 25 mL of boiling 5 M HCl, and the resulting solution was cooled, first to room temperature and then to 0 °C, whereupon a pale-yellow crystalline solid formed. This recrystallization procedure was repeated an additional two times affording a white crystalline solid. The final product was obtained by dissolution of the white solid in 5 M HCl with heating and then subsequent neutralization of the acidic solution by addition of 5 M NH_4OH . Upon neutralization, 4-(*p*-nitrophenyl)pyridine precipitated as a yellow crystalline solid, yield 1.36 g (34%). Mp: 120–122 °C (lit.²⁰ 124–125 °C). ^1H NMR (300 MHz, DMSO): δ 7.80 (d, $J = 6.0$ Hz, 2H, pyridyl), 8.07 (d, $J = 8.7$ Hz, 2H, phenyl), 8.34 (d, $J = 8.7$ Hz, 2H, phenyl), 8.70 (d, $J = 6.0$ Hz, 2H, pyridyl). ^{13}C NMR (75 MHz, DMSO): δ 122.0, 124.5, 128.6, 143.9, 145.1, 148.2, 150.9.

(b) *4-(p-Aminophenyl)pyridine (21)*.²⁰ A mixture of 4-(*p*-nitrophenyl)pyridine (435 mg, 2.1 mmol), iron powder (hydrogen reduced, 325 mesh, 2.4 g, 42 mmol), 0.2 mL of 5 M aqueous HCl, 40 mL of EtOH, and 2 mL of H_2O was heated to reflux under a blanket of N_2 for 2 h. The resulting mixture was filtered through a large-diameter short column of silica gel eluting with $\text{CH}_3\text{CN}-\text{CH}_2\text{Cl}_2$ 1:1 v/v. Collection of the eluant was monitored by TLC. After evaporation of solvent from fractions that contained the product, **21** was obtained as a yellowish crystalline

solid, yield 330 mg (92%). Mp: 228–232 °C (lit.²⁰ 227–228). ¹H NMR (300 MHz, DMSO): δ 5.52 (br, 2H, NH₂), 6.68 (d, $J = 8.7$ Hz, 2H, phenyl), 7.54 (d, $J = 8.7$ Hz, 2H, phenyl), 7.56 (d, $J = 6.0$ Hz, 2H, pyridyl), 8.49 (d, $J = 6.0$ Hz, 2H, pyridyl). ¹³C NMR (75 MHz, DMSO): δ 114.5, 119.8, 121.5, 127.8, 147.6, 150.3, 150.6.

erythro-1-(4-(4-Pyridyl)anilino)-2-piperidino-1,2-diphenylethane (e-2). The synthesis of this compound followed the general procedure described above for **e-1**, except **21** was added in place of 4-aminobenzonitrile. The crude product was purified by chromatography (silica, ethyl acetate–hexane 1:1 v/v). Product **e-2** was obtained as a yellow solid, yield 31% after purification. TLC (silica, ethyl acetate–hexane 50:50 v/v): $R_f = 0.4$. ¹H NMR (300 MHz, CDCl₃): δ 1.36 (m, 2H, pip), 1.47 (m, 4H, pip), 2.36 (br, 4H, pip), 3.40 (d, $J = 5.4$ Hz, 1H, benzylic), 4.75 (d, not well resolved, 1H, benzylic), 5.16 (s, 1H, NH), 6.48 (d, $J = 8.1$ Hz, 2H), 6.8–7.1 (m, 12H), 7.29 (d, not well resolved, 2H, pyridyl), 8.42 (d, $J = 4.8$ Hz, 2H, pyridyl).

meso-1,2-Dipiperidino-1,2-diphenylethane (m-4). **e-20** (1.0 g, 3.6 mmol) was dissolved in 10 mL of freshly distilled CH₂Cl₂, and triethylamine (1.5 mL, 11 mmol) was added. The mixture was purged with N₂ for 30 min, and at the same time the temperature was adjusted to –20 °C with a dry ice–2-propanol bath. A solution of methanesulfonyl chloride (0.28 mL, 3.6 mmol) dissolved in 2 mL of freshly distilled CH₂Cl₂ was added dropwise with the aid of a syringe. The resulting mixture was stirred at low temperature (–10 °C) for 1 h, whereupon piperidine (0.35 mL, 3.6 mmol) dissolved in 2 mL of CH₂Cl₂ was added dropwise. The reaction was discontinued after 1.5 h of stirring at low temperature. The CH₂Cl₂ solution was washed twice with H₂O, dried with Na₂SO₄, and concentrated to dryness. Product **m-4** was obtained as a white crystalline solid without further purification, yield 1.19 g (93%). TLC (silica gel, hexane–ethyl acetate 8:2 v/v): $R_f = 0.7$. ¹H NMR (300 MHz, CDCl₃): δ 1.10 (m, 4H, piperidine), 1.24 (m, 2H), 2.16 (m, 2H), 2.35 (m, 2H, piperidine), 4.15 (s, 1H, benzylic), 7.2–7.4 (m, 10H, phenyl). ¹³C NMR (75 MHz, CDCl₃): δ 24.6, 26.4, 50.5 (all piperidine), 69.8 (benzylic), 126.1, 127.0, 129.2, 137.4 (all aromatic).

e-1 Photoproduct Isolation and Characterization. (a) **Irradiation and Photoproduct Isolation.** A solution of **e-1** in CH₃CN (140 mL, 3 mM) was placed into a quartz container equipped with a stir bar, and the container was degassed by bubbling with a steady stream of argon for 2 h. The resulting argon-degassed solution was irradiated by using a medium-pressure Hg arc lamp (450 W, contained in a quartz immersion well) for 30 min. The CH₃CN solution was concentrated under reduced pressure and cooled. Upon cooling, crystals of photoproduct-1 formed and were collected by suction filtration. The reaction mixture was evaporated to dryness, and the solid was redissolved in CHCl₃. The CHCl₃ solution was concentrated and cooled, whereupon crystals of photoproduct-2 formed and were collected by suction filtration. The CHCl₃ was evaporated, and the residue was subjected to preparative-scale TLC (Merck silica, 250 μ m). The residue was applied to the TLC plate as a solution in ethyl acetate, and the plate was developed using ethyl acetate–hexane (5:95 v/v). After development two strongly fluorescent bands were apparent on the TLC plate at mid- R_f : (1) **e-1** at $R_f \approx 0.6$; (2) photoproduct-3 at $R_f \approx 0.7$. The high- R_f band due to photoproduct-3 was scraped from the TLC plate, and the product was extracted from the silica using CHCl₃.

(b) **Photoproduct-1: Analysis and Identification (d,l-3).** ¹H NMR (300 MHz, DMSO): δ 4.81 (d, $J = 6.6$ Hz, 1H), 6.51 (d, $J = 8.7$ Hz, 2H), 6.94 (d, $J = 6.6$ Hz, 1H), 7.15 (t, 1H),

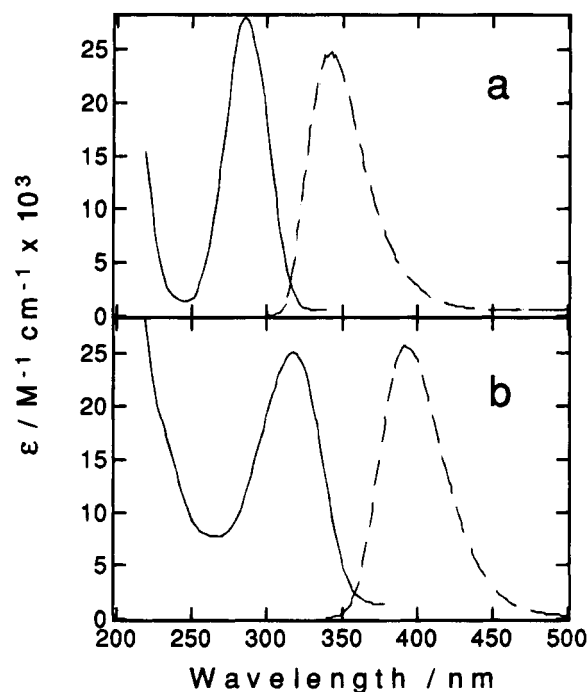


Figure 1. Absorption and fluorescence spectra of diamines in CH₃CN solution: solid lines, absorption; dashed lines, fluorescence; (a) **e-1**; (b) **e-2**.

7.24 (d, $J = 7.5$ Hz, 2H), 7.29 (d, $J = 8.7$ Hz, 2H), 7.47 (d, $J = 7.5$ Hz, 2H). ¹³C NMR (75 MHz, DMSO): δ 60.9, 96.8, 113.0, 120.6, 127.6, 128.0, 128.4, 133.5, 140.8, 151.2. FAB-HRMS calcd for C₂₈H₂₃N₄ (M + H) 415.1923, found 415.1909. The NMR spectra and mass analysis are consistent with structure **d,l-3**.

(c) **Photoproduct-2: Analysis and Identification (m-3).** ¹H NMR (300 MHz, DMSO): δ 4.68 (d, poorly resolved, 1H), 6.59 (d, $J = 8.7$ Hz, 2H), 7.08 (s, 5H), 7.34 (d, $J = 8.7$ Hz, 2H), 7.53 (d, poorly resolved, 1H). ¹³C NMR (75 MHz, DMSO): δ 62.1, 96.6, 113.2, 120.7, 127.4, 128.0, 128.3, 133.5, 140.5, 151.7. ¹H NMR (300 MHz, CDCl₃): δ 4.66 (d, poorly resolved, 1H), 4.95 (d, poorly resolved, 1H), 6.51 (d, $J = 8.7$ Hz, 2H), 7.08 (m, 2H), 7.3 (m, 5H), 7.34 (d, $J = 8.7$ Hz, 2H). FAB-HRMS calcd for C₂₈H₂₃N₄ (M + H) 415.1923, found 415.1914. The NMR spectra and mass analysis are consistent with structure **m-3**.

(d) **Photoproduct-3: Analysis and Identification (t-1).** The ¹H and ¹³C NMR spectra of this product are identical to those of an independently synthesized sample of **t-1** (see above). HRMS calcd for C₂₆H₂₈N₃ (M + H) 382.2283, found 382.2320. The NMR spectra and mass analysis are consistent with structure **t-1**.

(e) **Identification of m-4 and d,l-4 in Photoproduct Solution.** The existence of **m-4** in the photoproduct solution was confirmed by comparison of HPLC retention times of a known sample with the chromatogram of the photoreaction mixture. An authentic sample of **m-4** reproducibly gave a retention time of 31.5 min under the same HPLC conditions used for analysis of the reaction mixture. This retention time matched perfectly with the second peak of the “doublet” with longest retention time in the chromatogram of the reaction mixture (see Figure 2). The first peak of the long retention time “doublet” in the chromatogram of the reaction mixture was tentatively identified as **d,l-4** on the basis of the fact that it exhibits very similar retention time and area compared to the peak attributed to **m-4**.

(f) **Identification of 5 in Photoproduct Solution.** The existence of **5** in the photoproduct solution was confirmed by comparison

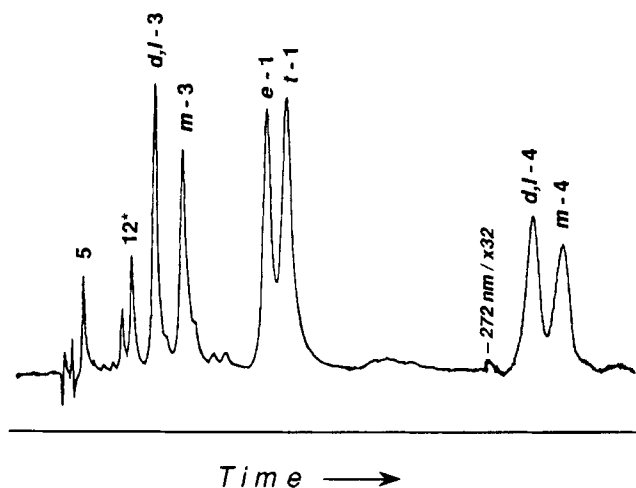


Figure 2. Reversed phase HPLC chromatogram of reaction mixture following irradiation of *e-1* (>75% conversion) in argon-degassed CH₃CN. Detector wavelength 290 nm and relative sensitivity $\times 1$ for most of chromatogram; detector wavelength changed to 272 nm and $\times 32$ relative sensitivity at point marked 272 nm/ $\times 32$ in chromatogram. Peaks are labeled according to identity of component; asterisk indicates that the identity of the component has not been confirmed by comparison of the retention time with that of an authentic sample.

of HPLC retention times of a known sample with the chromatogram of the photoreaction mixture. An authentic sample of **5** reproducibly gave a retention time of 3.7 min under the same HPLC conditions used for analysis of the reaction mixture.

General Procedures for Quantitative Photolyses. Quantum yield studies were carried out using a 75 W high-pressure Hg lamp housed in an elliptical reflector housing (PTI ALH-1000). The output from the 75 W lamp was passed through a grating monochromator and focused into a small compartment which contained the sample cell. The light intensity was determined twice each working day by using the Aberchrome 540 actinometer. HPLC was carried out on a system that was comprised of a Waters isocratic pump, a Valco injector, a ABI variable-wavelength absorption detector, a Hewlett-Packard integrating recorder, and a Whatman reversed phase analytical column (25 cm \times 4.6 mm, ODS-3). The mobile phase was comprised of CH₃CN–H₂O 40:60 v/v with 0.01 M sodium 1-heptanesulfonate and 0.025 M triethylamine. The detector wavelength was 286 nm for analysis of *e-1* and *t-1* and 320 nm for analysis of *e-2*. Identities of peaks in the chromatograph were established by comparison of retention times with authentic samples. Standard solutions were used to determine the calibration factors for components in the photoproduct mixture. Each calibration factor and Φ value is an average of measurements on four independently prepared and/or photolyzed solutions, and each solution was analyzed by triplicate injections into the HPLC. Solutions were degassed by bubbling with Argon for 30 min prior to irradiation.

The following is an example of the procedure followed for quantum efficiency measurements on *e-1*. A 3 mL aliquot of a degassed acetonitrile solution containing *e-1* (0.0005 M) was irradiated (313 nm, 75 W Hg lamp) for 7 min. Following light exposure, 0.5 mL of an internal standard solution (acetophenone 0.015 M in H₂O–CH₃CN 10:90 v/v pH = 3) was added to 2 mL of the photoproduct solution, and the mixture was analyzed by triplicate injections into the HPLC.

Methods for Emission, Transient Absorption, and Electrochemical Experiments. Time-resolved emission, transient absorption, steady-state emission, and electrochemistry were carried out by using methods and equipment that has been described in previous publications.^{14,15} All transient absorption

TABLE 1: Photophysical Properties^a

compound	absorption		fluorescence	
	λ_{\max}	$10^{-4}\epsilon_{\max}/M^{-1} \text{ cm}^{-1}$	λ_{\max}	τ^b/ns
<i>e-1</i>	286	2.8	346	0.4
<i>t-1</i>	286	2.8	346	0.4
5	272	2.3	336	3.1
6	284	2.7	346	3.1
<i>e-2</i>	318	2.5	392	1.1
9	306	2.2	386	2.0

^a All data for CH₃CN solutions at 298 K. ^b Estimated error ± 0.2 ns.

experiments were carried out by using a recirculating cell with a 100 mL volume to minimize the effects of sample decomposition during data acquisition.

Results

Structures. This study focuses on the photophysics and photochemistry of 1,2-diamines that contain a chromophore with substantial intramolecular charge transfer character. Two categories of chromophores have been examined, one based on the *p*-aminobenzonitrile (ABN) unit and another based on the 4-(*p*-aminophenyl)pyridine (APP) unit. The structures of the various ABN and APP diamines and model compounds are provided in Chart 1. Each 1,2-diamine exists as two diastereomers (see Chart 1), and throughout the manuscript, the prefixes *e*-, *t*-, *m*-, and *d,l*- refer to *erythro*-, *threo*-, *meso*-, and *d,l*- diastereomers, respectively. The photophysical and photochemical studies focus on diamines *e-1*, *t-1*, and *e-2*, while compounds **5**–**8** serve as models for the ABN chromophore and **9** and **10** serve as models for the APP chromophore.

Photophysics. Absorption spectra, emission spectra, and emission decay lifetimes were determined for several of the compounds shown in Chart 1 in CH₃CN solution (Table 1). The absorption and emission spectra of *e-1* and *e-2* shown in Figure 1 are typical for this series. Each ABN and APP compound exhibits a comparatively strong absorption band ($\epsilon \approx 2\text{--}3 \times 10^4 M^{-1} \text{ cm}^{-1}$) in the UV. This absorption is assigned to the ¹LE transition (long axis polarized) and is associated with substantial charge transfer from the amino donor into the benzonitrile (or phenylpyridine) π orbital system.^{6,12} Each compound also exhibits a structureless fluorescence with only a slight Stokes shift, which is attributed to radiative decay from the ¹LE state. None of the ABN or APP diamines exhibit a long-wavelength "TICT" emission in CH₃CN as observed for the extensively studied compound **8**.^{6,7,12,13} This leads to the conclusion that the excited state which is responsible for the long-wavelength emission of **8** is not involved in the photophysics or photochemistry of the ABN or APP diamines that are the focus of the present investigation.

The fluorescence lifetimes of ABN model compounds **5** and **6** are experimentally indistinguishable (3.1 ns). This lifetime reflects the rate of normal radiative and nonradiative decay of the ¹LE state of the ABN chromophore. By contrast, the fluorescence lifetimes of ABN-based diamine compounds *e-1* and *t-1* are substantially shorter (0.4 ns). A similar pattern is observed upon comparison of the fluorescence lifetimes of the two APP compounds: the lifetime of APP diamine *e-2* (1.1 ns) is reduced compared to that of the APP model compound **9** (2.0 ns). The reduced fluorescence lifetime for diamines *e-1*, *t-1*, and *e-2* is likely due to a nonradiative decay pathway that is associated with the presence of the piperidine tertiary amine donor site which accelerates the decay of the ¹LE state of the ABN or APP chromophore. This additional nonradiative decay pathway is likely intramolecular electron transfer from the piperidine donor to the excited ABN or APP unit (see below).

TABLE 2: Photochemical Quantum Yields^a

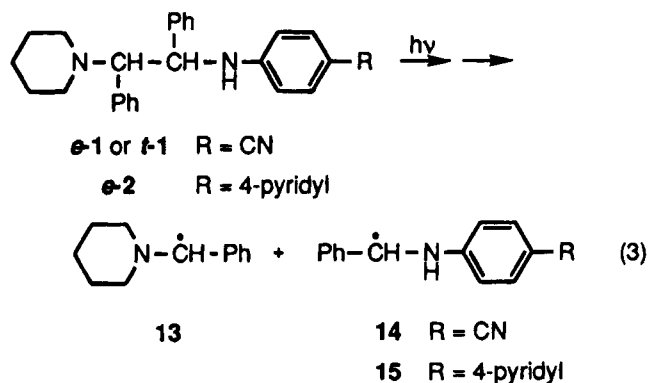
compound	air-saturated solution			argon-degassed solution		
	Φ^-	Φ^+_{isomer}	Φ^+_{amine}	Φ^-	Φ^+_{isomer}	Φ^+_{amine}
<i>e-1</i>	0.155 ± 0.015	0.026 ± 0.002	0.089 ± 0.004	0.105 ± 0.003	0.062 ± 0.004	0.020 ± 0.003
<i>t-1</i>	0.105 ± 0.007	0.018 ± 0.004	0.075 ± 0.004	0.065 ± 0.01	0.025 ± 0.003	0.020 ± 0.003
<i>e-2</i>	0.118 ± 0.01	0.016 ± 0.002	0.080 ± 0.004	0.065 ± 0.004	0.035 ± 0.01	0.011 ± 0.002

^a All data for CH₃CN solutions at 298 K. Φ^- , quantum efficiency for disappearance of starting material; Φ^+_{isomer} , quantum efficiency for formation of corresponding diastereomer; Φ^+_{amine} , quantum efficiency for formation of **5** (*e-1* or *t-1*) or **9** (*e-2*). All quantum efficiencies are averages of greater than or equal to three independent determinations, and the listed errors are the standard deviations in the averages.

predominates ($\Phi^+_{\text{isomer}} > \Phi^+_{\text{amine}}$). Third, *e-1* undergoes reaction with greater efficiency compared to *t-1* ($\Phi^-_{e-1} > \Phi^-_{t-1}$).

The photochemical reactivity of *e-2* was not explored in the same detail as for ABN diamines *e-1* and *t-1*; products were not isolated by preparative-scale photolysis in this system. However, HPLC coinjection confirmed the identity of the free amine photoproduct **9** in the chromatograms of reaction mixtures (Figure 4), and by analogy to the HPLC characteristics observed for *e-1* and *t-1*, the chromatographic peak that appears at slightly longer retention time compared to that of *e-2* is attributed to the diastereomeric compound *t-2*. Quantum efficiencies for disappearance of *e-2* (Φ^-) and for formation of free amine **9** and diastereomer *t-2* were determined for photolysis in air-saturated and argon-degassed CH₃CN (Table 2). As can be seen from these data, in every respect the reactivity of *e-2* is virtually identical to that of *t-1*.

At this point it is appropriate to point out that the steady-state photochemistry of *e-1*, *t-1*, and *e-2* is consistent with a mechanism in which the primary photochemical process leads to homolytic bond fragmentation of the 1,2 C–C bond. As shown in eq 3, photoinduced bond homolysis of *e-1* or *t-1* would



lead to formation of α -amino radicals **13** and **14**, while bond homolysis of *e-2* would lead to α -amino radicals **13** and **15**. In argon-degassed solution, random recombination of these radicals would lead to the observed products, and in air-saturated solution the observed products would be formed by oxidation of the primary radicals followed by hydrolysis. A thorough discussion of the steps leading to C–C bond fragmentation will be provided in the Discussion.

Transient Absorption Spectroscopy. Transient absorption spectroscopy was carried out on *e-1*, *t-1*, and *e-2* in an effort to determine the spectroscopic properties and dynamics of the reactive intermediates formed by photolysis. All experiments were carried out using the fourth harmonic of a Q-switched Nd:YAG laser for excitation (266 nm, 5 mJ/pulse, 10 ns fwhm). Samples were contained in a recirculating flow cell to minimize the effect of sample decomposition during data acquisition.

Figure 5a illustrates the transient absorption spectra of *e-1* and *t-1* in argon-degassed CH₃CN at 5 μ s delay after laser excitation. These spectra are identical to those observed

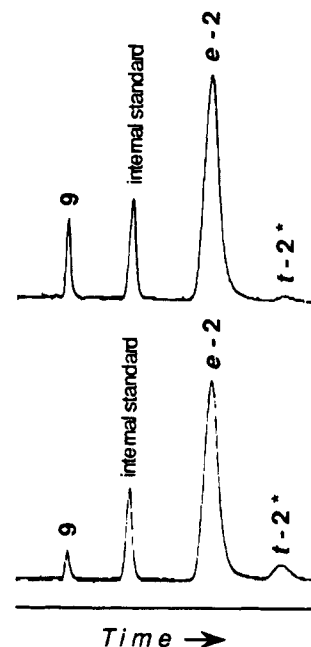


Figure 4. Reversed phase HPLC chromatogram of reaction mixture following irradiation of *e-2* ($\approx 10\%$ conversion) in CH₃CN. Detector wavelength 320 nm. Peaks are labeled according to identity of component; asterisk indicates that the identity of the component has not been confirmed by comparison of the retention time with that of an authentic sample. Top: air-saturated. Bottom: Argon degassed.

immediately following the laser pulse, which indicates that the transients that are responsible for the absorption are formed rapidly (< 20 ns). For both *e-1* and *t-1* the transient absorbance decays via second-order kinetics with $t_{1/2} \approx 150$ μ s. Identical transient absorption spectra are observed for *e-1* and *t-1* in air-saturated solution at 20 ns delay following laser excitation. However, in this case the transient absorbance decays by first-order kinetics with $\tau = 100$ ns. The diminished lifetime of the transient(s) formed by laser excitation of *e-1* and *t-1* in air-saturated solution is due to a pseudo-first-order reaction between the transient(s) and O₂. Assuming that [O₂] = 1.9 mM in air-saturated CH₃CN,²¹ the observed transient absorption decay lifetime indicates that the reactive intermediates are quenched by O₂ at $k_q \approx 5 \times 10^9$ M⁻¹ s⁻¹, which is very close to the diffusion-controlled limit in CH₃CN.

The behavior of the near-UV-absorbing reactive intermediates that are formed via pulse excitation of *e-1* and *t-1* strongly suggests that they can be assigned to the pair of α -amine radicals **13** and **14** (eq 3) that are formed by photoinduced C–C bond homolysis. An important feature is that the transient absorption produced by flash excitation of *e-1* is approximately 50% more intense compared to that of *t-1*. This observation is significant, because the two samples had matched absorbance at 266 nm and the experiments were carried out at identical laser power. This result indicates that α -amine radicals **13** and **14** are formed more efficiently from *e-1*, consistent with the steady-state

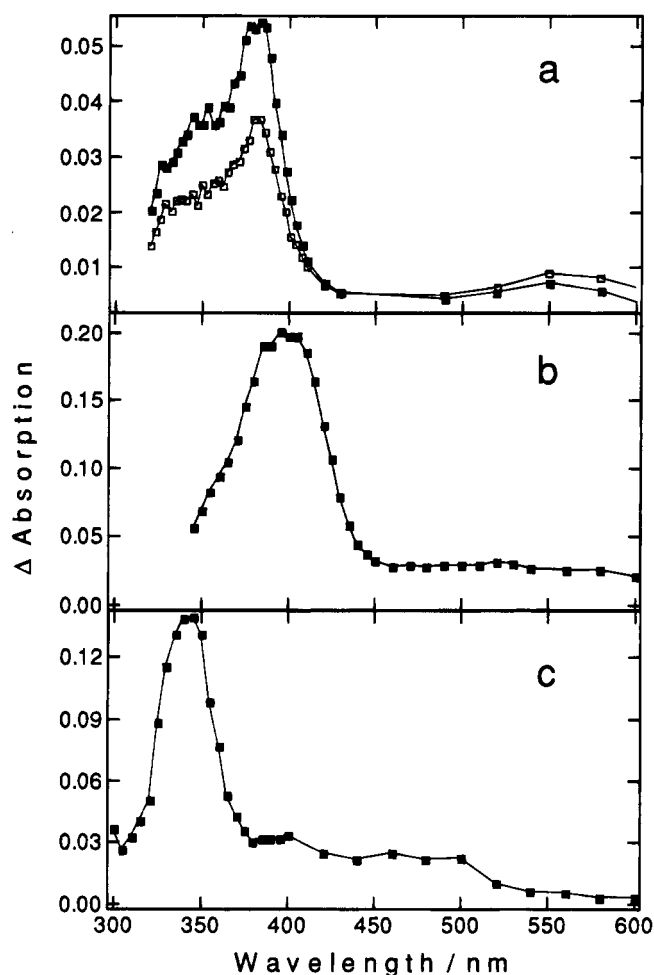


Figure 5. Transient absorption difference spectra following pulsed laser excitation (10 ns pulse width, dose = 5 mJ/pulse). All spectra are for samples in argon-degassed CH_3CN solution at 5 μs delay from the laser excitation pulse. Each sample was prepared so that the optical density was ca. 0.6 at the excitation wavelength: (a) *e-1*, filled squares; *t-1*, open squares; excitation wavelength 266 nm. (b) *e-2*; excitation wavelength 266 nm. (c) [(2,2'-bipyridine) $\text{Re}^{\text{I}}(\text{CO})_3(4\text{-benzylpyridine})$][PF_6] ($c = 7 \times 10^{-5}$ M) and diamine *m-4* ($c = 4$ mM); excitation wavelength 355 nm.

quantum yield data (Table 2), which shows *e-1* reacts approximately 50% more efficiently than *t-1*.

The transient absorption of *e-2* in argon-degassed CH_3CN at 5 μs following 266 nm excitation is illustrated in Figure 5b. This spectrum is identical to that observed immediately following the laser pulse, again indicating that the transient(s) responsible for the absorption is formed very rapidly (<20 ns). The transient absorption shown in Figure 5b decays via second-order kinetics with $t_{1/2} \approx 150 \mu\text{s}$. In air-saturated solution, the same transient absorption is observed at 20 ns delay following laser excitation; however, under these conditions the transient(s) are quenched by O_2 and the absorption decays via a rapid first-order process with $\tau \approx 100$ ns. It is clear that the overall properties of the transient(s) produced by flash excitation of *e-2* are parallel to those observed for *e-1* and *t-1*. By analogy it is likely that the transient absorption produced by pulse excitation of *e-2* can be attributed to α -amine radicals **13** and **15** that would be formed by photoinduced C–C bond homolysis of *e-2*.

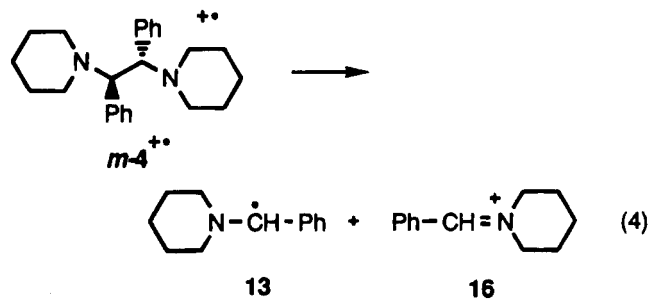
In an effort to obtain further information concerning the absorption properties of the α -amino radicals that are produced by photoinduced C–C bond homolysis in *e-1*, *t-1*, and *e-2*, an experiment was carried out which allowed exclusive formation

TABLE 3: Anodic Peak Potentials for Selected Compounds^a

compound	E_p^a/V
ABN Model Compounds	
5	+1.31
6	+1.30
7	+1.31 ^b
APP Model Compounds	
9	+1.07
10	+0.90 ^b
Piperidine Model Compound	
11	+0.97
Diamines	
<i>e-1</i>	+0.93
<i>t-1</i>	+0.98
<i>e-2</i>	+0.85
<i>m-4</i>	+0.80
<i>m-3</i>	+1.15

^a E_p^a is the peak potential for the first irreversible anodic wave. All measurements at Pt working electrode in $\text{CH}_3\text{CN}/0.1$ M tetrabutylammonium hexafluorophosphate, 200 mV sweep rate, concentration of analyte = 2 mM. Potentials are relative to saturated sodium chloride calomel reference electrode. ^b $E_{1/2}$ for reversible wave.

of α -amine radical **13**. Laser flash excitation (355 nm, 5 mJ/pulse, 10 ns fwhm) of an argon-degassed solution containing [(2,2'-bipyridine) $\text{Re}^{\text{I}}(\text{CO})_3(4\text{-benzylpyridine})$][PF_6] ($c = 7 \times 10^{-5}$ M) and diamine *m-4* ($c = 4$ mM) leads to formation of the diamine radical cation, *m-4*^{•+}, via bimolecular photoinduced electron transfer from *m-4* to the excited state $\text{Re}(\text{I})$ sensitizer.¹⁶ Following its production by bimolecular electron transfer, *m-4*^{•+} rapidly ($k \geq 10^8$ s⁻¹) undergoes C–C bond fragmentation to produce radical **13** and iminium ion **16**, eq 4. Figure 5c

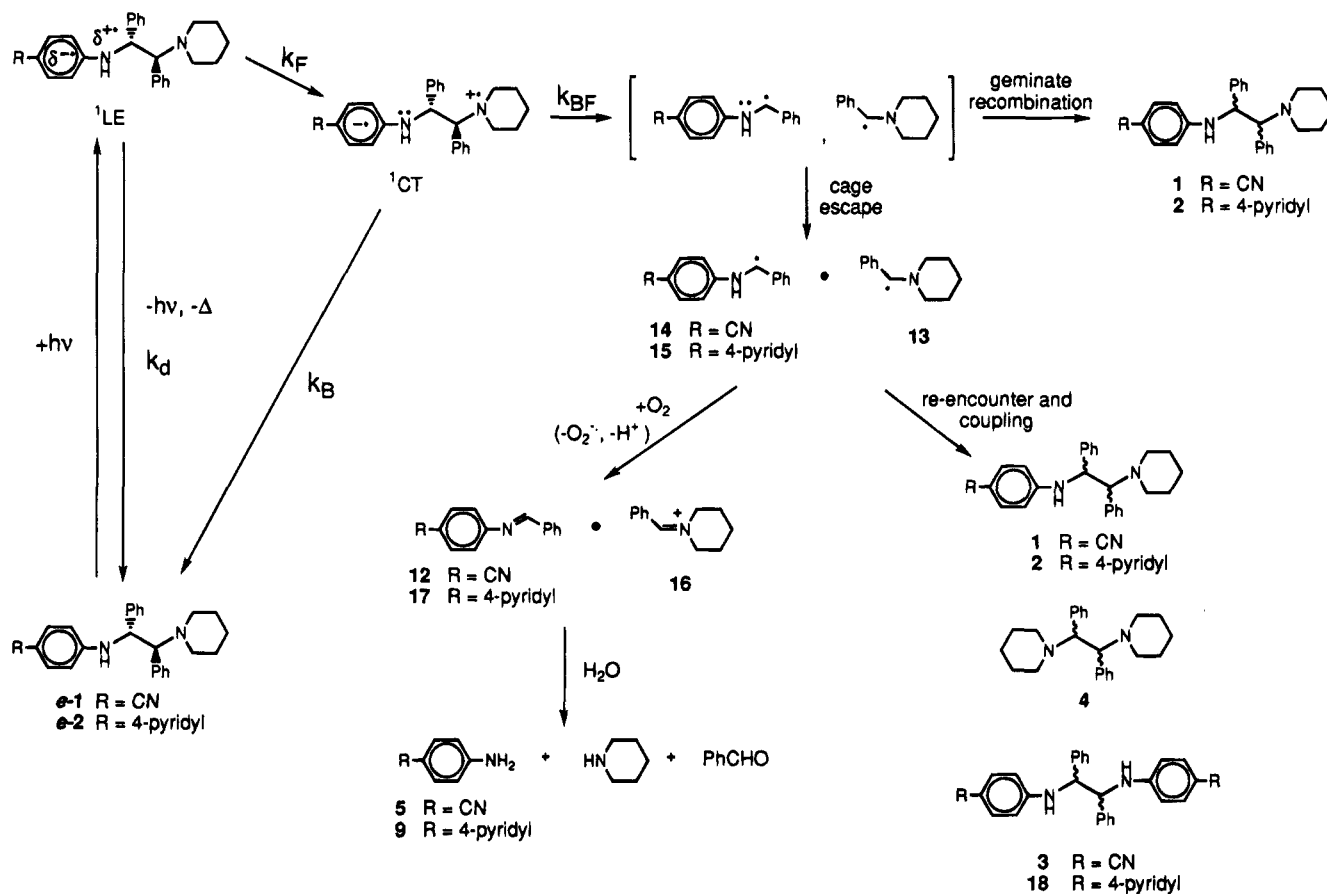


illustrates the transient absorption spectrum of the solution of *m-4* and the $\text{Re}(\text{I})$ complex taken 500 ns following the laser excitation pulse. The spectrum is dominated by a strong absorption band with $\lambda_{\text{max}} \approx 340$ nm with comparatively weaker absorptions that appear in the near-UV (370 nm) and into the visible (450–500 nm). The 340 nm absorption is due to radical **13** while the weaker near-UV and visible absorption bands are due to the reduced $\text{Re}(\text{I})$ metal complex.²² Consistent with assignment of the 340 nm band to **13**, this transient is quenched rapidly ($\tau < 100$ ns) when the bimolecular laser flash experiment is carried out in air-saturated solution.

Electrochemistry. Cyclic voltammetry was carried out on diamines *e-1*, *t-1*, and *e-2* as well as on a number of amine model compounds to determine the potentials for the first anodic process for each compound. At scan rates of 200 mV/s on solutions with 2 mM concentration, all of the compounds revealed an irreversible anodic wave with a peak potential that falls between +0.80 and +1.35 V vs SSCE (Table 3). Inspection of the data reveals several clear trends regarding the position of the anodic peak potentials (E_p^a).

First, the potentials for the various model compounds can be grouped into three categories. (1) For compounds that contain

SCHEME 2



only the ABN-type donor (e.g. 5–7), E_p^a occurs at approximately +1.30 V. This potential is consistent with that expected for oxidation of a cyano-substituted aniline.²³ Note that the peak potentials observed for 5 and 6 are similar to the half-wave potential for reversible oxidation of 7, which implies that the anodic peak potentials provide a good approximation of the thermodynamic potential for oxidation of the ABN moiety. (2) Compounds that contain only the APP-type donor (9 and 10) exhibit peak potentials between +0.9 and +1.1 V, which indicates that the APP-type aniline donor is more easily oxidized compared to the ABN-type aniline. (3) The peak anodic potential for tertiary aliphatic amine 11, which serves as a model for the piperidine donor, is +0.97 V. This potential is in accord with literature values for peak potentials of tertiary aliphatic amines in CH_3CN solution.²³

Second, ABN-type diamines *e-1* and *t-1* exhibit an anodic peak potential that is qualitatively in accord with the anodic potential of piperidine model 11. Importantly, the potential for *e-1* and *t-1* is substantially lower relative to that of the ABN model compounds 5–7 and the symmetric ABN diamine *m-3*. These observations imply that (1) the first oxidation of *e-1* and *t-1* (and therefore the HOMO) is localized largely on the piperidine tertiary amine nitrogen and not on the ABN unit and that (2) the piperidine-based HOMO of *e-1* and *t-1* lies 0.2–0.3 eV lower in energy than the highest orbital that is localized on the ABN unit.

Finally, for the APP diamine *e-2*, the anodic peak potential is lower than for APP models 9 or 10. Thus, it seems likely that in *e-2* the first oxidation, and therefore the HOMO, is also localized largely on the piperidine tertiary amine nitrogen. However, because the anodic peak potentials for the APP models are not significantly more positive than the potential of piperidine model 11, the situation concerning the nature of the

HOMO for this system is somewhat more equivocal than for the ABN-type diamines.

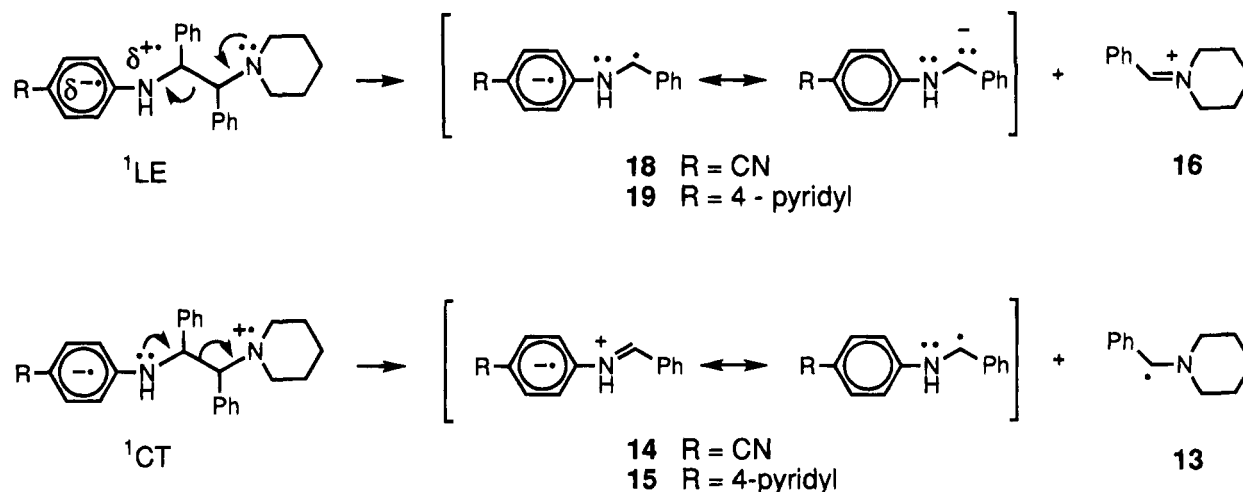
Discussion

Overall Mechanism of Photoreaction. All of the available results are consistent with the overall mechanism presented in Scheme 2. Aspects of this mechanism will be discussed in the sections that follow, but a brief synopsis is as follows. Photochemical excitation of the ABN or APP chromophore initiates homolytic C–C bond fragmentation. Following C–C bond homolysis, the resulting pair of α -amino radicals undergoes geminate recombination in competition with escape from the solvent cage. In argon-degassed solution, the free α -amino radicals decay primarily by recombination of radical pairs formed by random encounters. In air-saturated solution, the free α -amino radicals are oxidized rapidly by O_2 (see below), and the final product distribution is dominated by the hydrolyzed oxidation products. An important feature is the observation of *erythro* \rightarrow *threo* (or *threo* \rightarrow *erythro*) isomerization even in air-saturated solution, which strongly implies that geminate radical recombination occurs.

Excited States and Mechanism of Bond Fragmentation.

The similarity of the absorption and fluorescence spectra of diamines *e-1*, *t-1*, and *e-2* with the corresponding model ABN and APP compounds indicates that the excited state that is initially reached upon photoexcitation is 1LE .^{6,12} However, the fluorescence lifetimes of the diamines are diminished relative to the lifetimes of the corresponding ABN and APP models. This reduction in lifetime of 1LE is attributed to intramolecular electron transfer from the tertiary piperidine amine donor to the ABN or APP chromophore to form the 1CT state (k_F , Scheme 2).

SCHEME 3



Assuming that complete charge transfer occurs from the piperidine donor to the ABN or APP acceptor in 1CT , the free energy difference between 1LE and 1CT can be estimated by the expression²⁴

$$\Delta G_{^1LE \rightarrow ^1CT} = E^\circ(D/D^{+\bullet}) - E^\circ(A/A^{\bullet-}) - E_{^1LE}^{\circ-\circ} + \left(\frac{14.45}{\epsilon R_{DA}} \right) \quad (5)$$

where $E^\circ(D/D^{+\bullet})$ and $E^\circ(A/A^{\bullet-})$ represent the thermodynamic potentials for oxidation of the piperidine donor and reduction of the ABN or APP acceptor unit, respectively, and $E_{^1LE}^{\circ-\circ}$ is the energy of 1LE . The last term in eq 5 accounts for the electron-hole Coulombic stabilization in the 1CT state. Assuming $R_{DA} \approx 4 \text{ \AA}$ for the diamines, the Coulombic term is $\approx +0.1 \text{ eV}$ in CH_3CN solution. An estimate for $E^\circ(D/D^{+\bullet})$ in *e-1*, *t-1*, and *e-2* is $+0.90 \text{ V}$ on the basis of the peak potentials for model compounds **11** and *m-4*. Owing to the large negative potentials required for reduction of the ABN or APP units, reliable values for these potentials are not easily accessible. A literature value is available for the reduction potential of the ABN unit in DMF solution, $E^\circ(8/8^{\bullet-}) \approx -2.40 \text{ V}$.¹² The reduction potential of the APP chromophore is unavailable; however, potentials of analogous compounds suggest that $E^\circ(9/9^{\bullet-}) \approx -2.3 \text{ V}$.²³ The $E_{^1LE}^{\circ-\circ}$ values for the two chromophores are estimated from the position of the fluorescence maxima of appropriate model compounds as $E_{^1LE}^{\circ-\circ}(\text{ABN}) \approx +3.7 \text{ eV}$ and $E_{^1LE}^{\circ-\circ}(\text{APP}) \approx +3.2 \text{ eV}$. On the basis of these estimates $E_{^1LE}^{\circ-\circ} \approx -0.5$ and -0.1 eV for *e-1* and *e-2*, respectively. These energetic estimates establish that, for *e-1*, *t-1*, and *e-2*, 1CT is energetically below 1LE and is the likely explanation for the reduced lifetime of 1LE . Furthermore, the estimates imply that the $^1LE \rightarrow ^1CT$ transition in *e-2* is less exothermic compared to the analogous process in *e-1* and *t-1*.

Further evidence in favor of the involvement of 1CT in the fragmentation of *e-1*, *t-1*, and *e-2* comes from the observed mode of bond fragmentation. Photoinduced fragmentation of the ABN and APP diamines is believed to occur by analogy to the fragmentation of radical cations of 1,2-diamines, which occurs formally by a heterolytic process (see eq 1). In effect, photoexcitation of the ABN or APP chromophore withdraws electron density from the diamine functionality, thereby triggering C–C bond fragmentation. With this in mind, different outcomes are expected if C–C bond fragmentation occurs in 1LE or 1CT . As illustrated in Scheme 3, a formally heterolytic

bond fragmentation in 1LE would produce an ion pair (e.g., **18** or **19** paired with **16**), while an analogous process in 1CT would produce a radical pair (e.g., **14** or **15** paired with **13**). All of the available experimental data are consistent with the formation of the radical pair by the primary C–C bond fragmentation (see below), consistent with assignment of the reactive excited state to 1CT .

Structure and Spectra of α -Amino Radicals Produced by Bond Fragmentation. The model presented in Scheme 2 presumes that an unsymmetrical pair of α -amino radicals (e.g., **14** and **13** or **15** and **13**) is formed via photoinduced homolytic bond fragmentation of diamines *e-1*, *t-1*, and *e-2*. If this is indeed the case, then the transient absorption spectra shown in Figure 5a and b must be composed of the superimposed spectra of the individual α -amino radicals.

The transient absorption spectra of *e-1* and *t-1* (Figure 5a) exhibit a strong band with $\lambda_{\text{max}} \approx 382 \text{ nm}$ and a weaker shoulder in the 340–350 nm region. Independent generation of radical **13** reveals that this species exhibits a broad absorption centered at 345 nm (Figure 5c). This result suggests that the 340–350 nm shoulder in the transient absorption spectra of *e-1* and *t-1* is due to **13** and, by inference, that the more intense absorption at 382 nm is due to **14**. By contrast, the transient absorption spectrum of *e-2* appears as a single, intense absorption with $\lambda_{\text{max}} \approx 395 \text{ nm}$. It is very likely that this absorption is predominantly due to **15**. Unlike the case of the spectra for *e-1* and *t-1*, a shoulder is not observed at shorter wavelength in the transient absorption of *e-2*. However, the transient absorption intensity for *e-2* is substantially stronger than that for either isomer of **1**; therefore, it is possible that the strong absorption of **15** masks the weaker band due to radical **13**, which must be produced by fragmentation of *e-2* as well.

Radicals **13**–**15** have the common structural feature that they are α -amino-substituted benzylic radicals, $\text{Ph}\dot{\text{C}}\text{HNR}_2$.¹⁶ However, they differ in the pattern of substitution at the amine nitrogen: **13** features two alkyl substituents, while **14** and **15** bear a single aryl substituent. Interestingly, the transient absorption spectra in Figure 5 reveal that both the presence of the α -amino functionality and the pattern of N-substitution have a pronounced effect upon both the absorption maximum and absorption intensity (molar absorptivity) of these benzylic radical species. For comparison purposes, the parent (unsubstituted) benzyl radical exhibits an absorption at 320 nm ($\epsilon \approx 8800 \text{ M}^{-1} \text{ cm}^{-1}$).²⁵ Thus, substitution of the *N,N*-dialkylamine at the α -carbon induces a 25 nm red-shift of the absorption of the benzyl radical with a concomitant increase in the oscillator

strength.¹⁶ Furthermore, an even more substantial red-shift and increase in oscillator strength is induced when the α -amine bears an aryl substituent—compared to the absorption of the parent benzyl radical, 60 and 80 nm red-shifts are observed for radicals **14** and **15**, respectively. These substantial red-shifts very likely are due to delocalization of the unpaired spin-density into the N-aryl substituent as exemplified by the zwitterionic “resonance” structures shown for **14** and **15** in Scheme 3. Note that the absorption of **15** is more red-shifted compared to that of **14**, which is consistent with the possibility for a greater degree of delocalization into the aryl group in the former radical.

Reactivity of α -Amino Radicals Produced by Photofragmentation. The steady-state and time-resolved photochemical experiments provide a good description of the reactivity of the α -amino radicals, Ph $\dot{\text{C}}\text{HNR}_2$, produced by fragmentation of the diamines. First, the product studies indicate that O₂ effectively oxidizes these species, and this observation is supported by the transient absorption data which demonstrate that the radicals react rapidly with O₂ ($k \approx 5 \times 10^9 \text{ M}^{-1} \text{ s}^{-1}$). Rapid electron transfer from α -amino radicals to O₂ is consistent with the fact that these radicals are strongly reducing in nature: electrochemical studies indicate that $E_{1/2}(\text{PhCH}=\text{N}^+\text{R}_2/\text{Ph}\dot{\text{C}}\text{HNR}_2) \approx -0.90 \text{ V vs SCE}$.²⁶

The second major reaction pathway followed by the α -amino radicals is recombination. All of the expected symmetrical and unsymmetrical recombination products are observed following irradiation of argon-degassed solutions. Furthermore, HPLC analysis of the product mixture obtained following extended irradiation of an argon-degassed solution (Figure 2) indicates that the ratios of each of the three diastereomeric pairs *m-3*:*d,l-3*, *e-1*:*t-1*, and *m-4*:*d,l-4* are near unity, suggesting that each recombination process occurs non-stereospecifically. The lack of stereospecificity in these recombination reactions is in accord with the results of previous studies involving the thermal decomposition of optically active azo compounds, which occurs with a complete loss of stereochemistry for both geminate and out of cage recombination reactions.^{27,28}

Random recombination does not occur in the presence of O₂ as a scavenger for the free α -amino radicals. However, the fact that *erythro* \rightarrow *threo* (or *threo* \rightarrow *erythro*) isomerization occurs in the presence of O₂ implies that geminate recombination takes place. If geminate recombination is non-stereospecific, then it is possible to utilize the experimental steady-state quantum efficiencies for air-saturated solution to evaluate the total quantum efficiency for bond fragmentation, Φ_{BF} , and the efficiency of recombination within the geminate radical pair, η_{gr} :

$$\Phi_{\text{BF}} = \Phi^- + \Phi^+_{\text{isomer}} \quad \eta_{\text{gr}} = \frac{2\Phi^+_{\text{isomer}}}{\Phi_{\text{BF}}} \quad (6)$$

These expressions are based on the idea that when geminate recombination occurs, 50% of the time, the diastereomer is formed and, 50% of the time, the starting material is regenerated. In effect, Φ^- is suppressed because geminate recombination sometimes leads to unproductive bond fragmentation events; therefore, Φ^+_{isomer} is added as a “correction” to provide the true value for Φ_{BF} . Using the experimental parameters for air-saturated solution, Φ_{BF} and η_{gr} were calculated for *e-1*, *t-1*, and *e-2*, and the values are listed in Table 4. For each isomer η_{gr} falls in the range 0.25–0.30, which is in excellent agreement with the efficiency for geminate recombination observed in the aforementioned studies of optically active azo compounds (0.28–0.30).^{27,28} This concordance lends credibility to the assumption that geminate recombination is non-stereospecific.

TABLE 4: Kinetic Parameters for Reactive Diamines^a

compound	Φ_{BF}	$k_{\text{F}}/10^9 \text{ s}^{-1}$	η_{CT}	η_{GR}	η_{BF}
<i>e-1</i>	0.18	2.0	0.87	0.28	0.20
<i>t-1</i>	0.12	2.0	0.87	0.30	0.14
<i>e-2</i>	0.13	0.4	0.45	0.25	0.29

^a Parameters derived as defined in text.

Kinetic Model for the Reactive Diamines. If the overall mechanism described in the preceding sections and summarized in Scheme 2 provides an accurate description of the excited states and reactive intermediates involved in the photochemistry and photophysics of the reactive diamines, it then becomes possible to develop a kinetic model that relates the experimental kinetic parameters to microscopic rate constants. Assuming that ¹LE is created with unit efficiency by photoexcitation, the first step of the proposed mechanism is intramolecular charge transfer to form ¹CT. The rate and efficiency of this process (k_{F} and η_{CT} , respectively) can be calculated by eqs 7 and 8,²⁴

$$k_{\text{F}} = \frac{1}{\tau_{\text{diamine}}} - \frac{1}{\tau_{\text{model}}} \quad (7)$$

$$\eta_{\text{CT}} = 1 - \frac{\tau_{\text{diamine}}}{\tau_{\text{model}}} \quad (8)$$

where τ_{diamine} and τ_{model} are, respectively, the fluorescence lifetimes of ¹LE in diamines *e-1*, *t-1*, and *e-2* and the appropriate model compounds (**5** and **9**). Within ¹CT, there is a dynamic competition between back electron transfer to the ground state and bond fragmentation to produce the geminate radical pair (k_{B} and k_{BF} , respectively). This competition is described by the parameter η_{BF} , which is the efficiency of bond fragmentation within ¹CT,

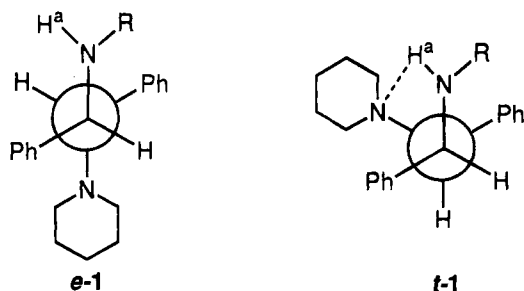
$$\eta_{\text{BF}} = \frac{k_{\text{BF}}}{k_{\text{BF}} + k_{\text{B}}} \quad (9)$$

Finally, in order to utilize all of the experimental parameters to estimate the microscopic rate constants, it is necessary to define the relationship between η_{CT} , η_{BF} , and the quantum efficiency for bond fragmentation (Φ_{BF}),

$$\Phi_{\text{BF}} = \eta_{\text{CT}}\eta_{\text{BF}} \quad (10)$$

By using eqs 7–10, k_{F} , η_{CT} , and η_{BF} were calculated for the reactive diamines, and the data are collected in Table 4. Several points are of interest with respect to these parameters. First, for all of the reactive diamines $\eta_{\text{CT}} > \Phi_{\text{BF}}$, which indicates that the process responsible for quenching of ¹LE occurs with substantially higher efficiency than bond fragmentation. While not an obvious point, this provides further support for involvement of an intermediate state (e.g., ¹CT) in bond fragmentation, since if fragmentation occurs directly from ¹LE (and is therefore directly responsible for quenching of ¹LE), then η_{CT} should be equivalent to Φ_{BF} . Second, the kinetic analysis implies that the difference in reactivity of *e-1* and *t-1* results from a difference in η_{BF} , because the rate and efficiency for formation of ¹CT (k_{F} and η_{CT}) are identical in the two diastereomers. Since η_{BF} defines the competition between bond fragmentation and back electron transfer, the observation that $\eta_{\text{BF}}^{e-1} > \eta_{\text{BF}}^{t-1}$ implies that $k_{\text{B}}^{e-1} < k_{\text{B}}^{t-1}$ and/or $k_{\text{BF}}^{e-1} > k_{\text{BF}}^{t-1}$ (refer to Scheme 2 for definition of rate constants). We favor the latter case (e.g., that bond fragmentation is faster in *e-1*) for reasons that will be discussed in the succeeding section. Finally, although it is

CHART 2



difficult to draw conclusions regarding the difference in reactivity of *e-1* and *e-2*, it is clear that one reason for the lower reactivity of the latter compound is that formation of ^1CT from ^1LE is less efficient in this system. Note that this is consistent with the thermodynamic analysis presented above that suggested that the driving force for the $^1\text{LE} \rightarrow ^1\text{CT}$ process is less exothermic in *e-2* compared to *e-1*.

Concerning the Difference in Reactivity of *e-1* and *t-1*. It is clear that *e-1* undergoes photofragmentation more efficiently than *t-1*. As a working hypothesis, we suggest that the increased reactivity of the *erythro* isomer is due to an enhanced rate of bond fragmentation ($k_{\text{BF}}^{e-1} > k_{\text{BF}}^{t-1}$) and that back electron transfer from ^1CT occurs at approximately the same rate in the two isomers ($k_{\text{B}}^{e-1} \approx k_{\text{B}}^{t-1}$). The hypothesis that $k_{\text{BF}}^{e-1} > k_{\text{BF}}^{t-1}$ is supported by previous studies of C-C bond fragmentation in 1,2-amino alcohol radical cations, in which it was observed that k_{BF} is greater for the *erythro* isomer.^{19,29}

The difference in k_{BF} for the two diastereomers may be linked to a difference in the energetically preferred conformations that the molecules adopt in the ground state. Evidence for these preferred conformations comes from the ^1H NMR spectra, which imply that in non-hydrogen-bond acceptor solvents *e-1* and *t-1* exist predominantly in the conformations shown in Chart 2. These conformational assignments are based on the chemical shift of the aryl amine proton (H^a , Chart 2) in the two diastereomers in the non-hydrogen-bond acceptor solvent CDCl_3 : amine proton H^a appears at 5.48 ppm in *e-1* and at 6.72 ppm in *t-1*. The substantial downfield shift of H^a in *t-1* is consistent with an intramolecular hydrogen bond between H^a and the piperidino nitrogen, as shown in Chart 2. Further evidence that the downfield shift in *t-1* is due to hydrogen bonding comes from the fact that the chemical shift of H^a is downfield and at virtually the same chemical shift for both diastereomers in the hydrogen-bond acceptor solvent DMSO (6.81 and 6.92 ppm in *e-1* and *t-1*, respectively). The similarity of the chemical shifts of H^a for the two isomers in DMSO is likely due to an intermolecular hydrogen bond between H^a and the solvent for both isomers.

The fact that $k_{\text{BF}}^{e-1} > k_{\text{BF}}^{t-1}$ can now be explained by reference to the conformations of the two diastereomers shown in Chart 2. The energetics of the reaction pathway for C-C bond fragmentation of radical cations that feature vicinal heteroatom substituents have been examined by using semiempirical and ab initio calculations.^{30,31} These calculations indicate that the vicinal heteroatom substituents are *anti* with respect to torsion about the central C-C bond in the energetically preferred reaction trajectory. The *anti* conformation is energetically favored because it allows maximum overlap between the lone pair orbitals (p-type) on the heteroatoms and the elongated, electron deficient C-C bonding orbital (σ -type) in the transition state for bond fragmentation. Now, as illustrated by Chart 2, NMR evidence suggests that the vicinal amino groups are *anti* in the preferred conformation of *e-1*, while they are *gauche* in the preferred con-

formation of *t-1*. This difference in conformation of the ground-state diastereomers may explain the difference in reactivity of the isomers in the photoexcited ^1CT state. The *erythro* isomer may react more rapidly because photoexcitation leads to production of ^1CT , in which the vicinal amino groups are *anti*, and this conformation facilitates C-C bond fragmentation.

Summary and Conclusions

Several 1,2-diamines that contain the ABN or APP chromophore undergo C-C bond fragmentation upon near-UV photoexcitation. The present study indicates that even though the ^1LE state of the ABN or APP chromophore is initially populated by optical excitation, the bond fragmentation reaction occurs from a lower lying ^1CT state that is formed by electron transfer from the piperidine tertiary amine donor to either the ABN or APP unit. The moderate-to-low efficiency for bond fragmentation arises because of competition at two stages of the excited-state reaction. First, there is a competition between formation of ^1CT from ^1LE by forward electron transfer and decay of ^1LE by radiative and nonradiative pathways. Second, there is a competition between bond fragmentation within ^1CT and nonradiative decay of ^1CT by back electron transfer. Analysis of the photochemical and photophysical information indicates that (1) the moderately exothermic forward electron transfer reaction between the piperidine donor and the excited-state ABN or APP chromophore occurs with $k_{\text{F}} \geq 5 \times 10^8 \text{ s}^{-1}$ for all of the molecules examined and that (2) bond fragmentation within ^1CT competes reasonably well with decay by back electron transfer (e.g., η_{BF} ranges from 0.15 to 0.30). Since ^1CT is not observed by nanosecond transient absorption, decay of ^1CT by back electron transfer occurs rapidly (e.g., $k_{\text{B}} \geq 10^8 \text{ s}^{-1}$). Therefore, since bond fragmentation within ^1CT is moderately competitive with back electron transfer, it follows that bond fragmentation is very rapid as well (e.g., $k_{\text{BF}} \geq 10^8 \text{ s}^{-1}$). The implication that C-C bond fragmentation is very rapid in the ^1CT state of these diamines is consistent with earlier work which suggested that the radical cations of 1,2-diamines fragment at rates exceeding 10^9 s^{-1} .^{16,18}

Acknowledgment. We gratefully acknowledge the National Science Foundation (Grant CHE 91-23000) for support of this work.

References and Notes

- (1) Nagakura, S.; Tanaka, J. *J. Chem. Phys.* **1954**, *22*, 236.
- (2) Lippert, E. *Z. Naturforsch.* **1955**, *10a*, 541.
- (3) Mataga, N.; Kaifu, Y.; Koizuma, M. *Bull. Chem. Soc. Jpn.* **1956**, *29*, 465.
- (4) Foster, R. *Organic Charge Transfer Complexes*; Academic Press: New York, 1969.
- (5) Mulliken, R. S.; Person, W. B. *Molecular Complexes*; Wiley-Interscience: New York, 1969.
- (6) Grabowski, Z. R.; Rotkiewicz, K.; Siemiarczuk, A.; Cowley, D. J.; Baumann, W. *Nouv. J. Chim.* **1979**, *3*, 443.
- (7) Rettig, W. *Angew. Chem., Int. Ed. Engl.* **1986**, *25*, 971.
- (8) Pasmán, P.; Mes, G. F.; Koper, N. W.; Verhoeven, J. W. *J. Am. Chem. Soc.* **1985**, *107*, 5839.
- (9) Hermant, R. M.; Bakker, N. A. C.; Scherer, T.; Krijnen, B.; Verhoeven, J. W. *J. Am. Chem. Soc.* **1990**, *112*, 1214.
- (10) Foley, M. J.; Singer, L. A. *J. Phys. Chem.* **1994**, *98*, 6430.
- (11) *Nonlinear Optical Properties of Organic Molecules and Crystals*; Chemla, D. S., Zyss, J., Eds.; Academic Press: Orlando, FL, 1987; Vols 1 and 2.
- (12) Leinhos, U.; Kuhnle, W.; Zachariasse, K. *J. Phys. Chem.* **1991**, *95*, 2013.
- (13) Zachariasse, K. A.; von der Haar, T.; Hebecker, A. *Pure Appl. Chem.* **1993**, *65*, 1745.

- (14) Wang, Y.; Hauser, B. T.; Rooney, M. M.; Burton, R. D.; Schanze, K. S. *J. Am. Chem. Soc.* **1993**, *115*, 5675.
- (15) Wang, Y.; Schanze, K. S. *Chem. Phys.* **1993**, *176*, 305.
- (16) Wang, Y.; Lucia, L. A.; Schanze, K. S. *J. Phys. Chem.* **1995**, *99*, 1961.
- (17) Kellett, M. A.; Whitten, D. G. *J. Am. Chem. Soc.* **1989**, *111*, 2314.
- (18) Leon, J. W.; Whitten, D. G. *J. Am. Chem. Soc.* **1993**, *115*, 8038.
- (19) Ci, X.; Kellett, M. A.; Whitten, D. G. *J. Am. Chem. Soc.* **1991**, *113*, 3893.
- (20) Katritzky, A. R.; Simmons, P. *J. Chem. Soc.* **1960**, 1511.
- (21) Murov, S. L.; Carmichael, I.; Hug, G. *Handbook of Photochemistry*; Marcel-Dekker: New York, 1993.
- (22) Lucia, L. A.; Schanze, K. S. *Inorg. Chim. Acta* **1994**, *225*, 41.
- (23) *Encyclopedia of the Electrochemistry of the Elements*; Bard, A. J., Ed.; Marcel Dekker: New York, 1973.
- (24) Oevering, H.; Paddon-Row, M. N.; Heppener, M.; Oliver, A. M.; Cotsaris, E.; Verhoeven, J. W.; Hush, N. S. *J. Am. Chem. Soc.* **1987**, *109*, 3258.
- (25) Claridge, R. F. C.; Fischer, H. *J. Phys. Chem.* **1983**, *87*, 1960.
- (26) Wayner, D. D. M.; Parker, V. D. *Acc. Chem. Res.* **1993**, *26*, 287.
- (27) Kopecky, K. R.; Gillan, T. *Can. J. Chem.* **1969**, *47*, 2371.
- (28) Greene, F. D.; Berwick, M. A.; Stowell, J. C. *J. Am. Chem. Soc.* **1970**, *92*, 867.
- (29) Lucia, L. A.; Burton, R. D.; Schanze, K. S. *J. Phys. Chem.* **1993**, *97*, 9078.
- (30) Bellvile, D. J.; Pabon, R. A.; Bauld, N. L. *J. Am. Chem. Soc.* **1985**, *107*, 4978.
- (31) Camaioni, D. M. *J. Am. Chem. Soc.* **1990**, *112*, 9475.

JP942493Y